

Chandra monitoring observations of the ultraluminous X-ray source NGC 5204 X-1

T. P. Roberts^{1*}, R. E. Kilgard^{1,2}, R. S. Warwick¹, M. R. Goad¹ & M. J. Ward³

¹ *X-ray and Observational Astronomy Group, Dept. of Physics & Astronomy, University of Leicester, University Road, Leicester, LE1 7RH*

² *Harvard-Smithsonian Center for Astrophysics, Cambridge, MA 02138, USA*

³ *Dept. of Physics, University of Durham, South Road, Durham DH1 3LE*

In prep.

ABSTRACT

We report the results of a 2-month campaign conducted with the *Chandra* X-ray observatory to monitor the ultraluminous X-ray source (ULX) NGC 5204 X-1. This was composed of a 50-ks observation, followed by ten 5-ks follow-ups spaced initially at ~ 3 , then at ~ 10 day intervals. The ULX flux is seen to vary by factors ~ 5 on timescales of a few days, but no strong variability is seen on timescales shorter than an hour. There is no evidence for a periodic signal in the X-ray data. An examination of the X-ray colour variations over the period of the campaign shows the ULX emission consistently becomes spectrally harder as its flux increases. The X-ray spectrum from the 50-ks observation can be fitted by a number of disparate spectral models, all of which describe a smooth continuum with, unusually for a ULX, a broad emission feature evident at 0.96 keV. The spectral variations, both within the 50-ks observation and over the course of the whole campaign, can then be explained solely by variations in the continuum component. In the context of an optically-thick corona model (as found in other recent results for ULXs) the spectral variations can be explained by the heating of the corona as the luminosity of the ULX increases, consistent with the behaviour of at least one Galactic black hole system in the strongly-Comptonised very high state. We find no new evidence supporting the presence of an intermediate-mass black hole in this ULX.

Key words: X-rays: galaxies - X-rays: binaries - Black hole physics

1 INTRODUCTION

Although ultraluminous X-ray sources (ULXs) were detected and studied by *Einstein* (e.g. Fabbiano 1989), *ROSAT* (e.g. Roberts & Warwick 2000; Colbert & Ptak 2002; Liu & Bregman 2005) and *ASCA* (e.g. Makishima et al. 2000), the *Chandra* and *XMM-Newton* observatories have provided us with the clearest view to date of these extraordinary X-ray sources (see e.g. Miller & Colbert 2004 for a review of the early results from these missions). However, despite the advances afforded by these missions over their predecessors, a concise determination of the underlying nature of ULXs has remained stubbornly elusive.

One certainty is that the high observed luminosities of ULXs ($L_X > 10^{39}$ erg s⁻¹) cannot be explained by stellar-mass black holes radiating isotropically below their Eddington limit. As this luminosity limit is directly proportional to the mass of the accreting object, the simplest solution is to turn to a new class of larger black holes, that we now refer to as “intermediate-mass” black holes (IMBHs; Colbert & Mushotzky 1999), with typical masses in the $10^2 - 10^4 M_\odot$ range. Such objects are certainly enticing as they would fill in a gap in the known mass range of black holes,

that currently falls between ~ 20 and $\sim 10^5 M_\odot$ (i.e. between the stellar-mass objects observed in our own Galaxy, and the supermassive black holes present in many galactic nuclei). However, there is not a single piece of evidence that currently establishes beyond doubt that any individual ULX contains an IMBH. A combination of factors - most notably its extreme luminosity - make M82 X-1 the best current candidate (e.g. Portegies-Zwart et al. 2004). Evidence that other bright ULXs contain IMBHs is provided largely by the detection of a soft excess in their X-ray spectrum, that can be fitted with an accretion disc spectrum with an inner disc temperature of $\sim 0.1 - 0.3$ keV, suggestive of the presence of an IMBH (Miller et al. 2003; Miller, Fabian & Miller 2004).

However, this last spectral interpretation has recently been challenged by new spectral data and modelling that questions the necessity for IMBHs to power even the most luminous ULXs (e.g. Stobbart, Roberts & Wilms 2006; hereafter SRW06). This complements the circumstantial evidence from multi-wavelength data - in particular the over-abundance of ULXs found in galaxies hosting very active star formation - that argues against IMBHs constituting a large fraction of the ULX population (King 2004). Additionally, the break in the X-ray luminosity function of ULXs at $\sim 2 \times 10^{40}$ erg s⁻¹ (Grimm, Gilfanov & Sunyaev 2003) is difficult to reconcile with black holes larger than $\sim 100 M_\odot$ contributing any-

* E-mail: tro@star.le.ac.uk

thing but a small minority of the ULX population. These arguments therefore support a demography in which the majority of the ULX population are a type of stellar-mass ($\sim 10 M_{\odot}$, though plausibly up to a few times larger) black hole X-ray binary that can match or even exceed its Eddington limit. Models for achieving super-Eddington luminosities from these systems include the “slim” disc model (e.g. Watarai, Mizuno & Mineshige 2001), radiation-pressure dominated discs (Begelman 2002), mildly-anisotropic radiation patterns from sources emitting at or below the Eddington limit (King et al. 2001) and relativistic beaming (Körding, Falcke & Markoff 2002).

Whilst concerted efforts have been made to understand the nature of ULXs via X-ray spectroscopy and multi-wavelength follow-up, variability characteristics (particularly in harness with spectroscopy) have not yet been as widely utilised. Yet, as *RXTE* has so spectacularly demonstrated, the key to understanding accreting sources is to study changes in their behaviour over a wide variety of timescales (cf. McClintock & Remillard 2006 for a review of the properties of Galactic black hole binaries). In fact, variability measurements over many different timescales could provide key measurements for understanding the nature of ULXs.

For example, the detection of a 3:2 ratio twin-peak high-frequency quasi-periodic oscillation (QPO) at ~ 1 Hz frequency from a ULX would imply the presence of an IMBH (Abromowicz et al. 2004; though we note that scaling arguments based on detections in Galactic black holes show that even a mission with the anticipated capabilities of *XEUS* is likely to struggle to detect such a signature). The detection of low-frequency QPOs may be less revealing, though several authors have estimated the mass of the black hole in M82 X-1 based on the frequency of a QPO detection, amongst other factors (e.g. Fiorito & Titarchuk 2004; Dewangan, Titarchuk & Griffiths 2006; Mucciarelli et al. 2006). A simpler argument based on this QPO, which is the best-detected example of this phenomenon in a ULX to date, is that its presence argues against geometric beaming of the X-ray flux in M82 X-1, implying that an IMBH is likely to be present (Strohmayer & Mushotzky 2003; though see Kaaret, Simet & Lang 2006b for caveats).

A second possible diagnostic for ULXs from short-timescale variability measurements is the shape of the fluctuation Power Spectral Density (PSD). In particular, the characteristic frequency of breaks in the PSD slope can be used to infer masses based on the assumption of a direct scaling of properties between Galactic black holes and AGNs (see e.g. Uttley et al. 2002). Cropper et al. (2004) used this technique to support the case that NGC 4559 X7 is a $> 1000 M_{\odot}$ IMBH (though they discuss alternatives). In contrast, Soria et al. (2004) examined the PSD of NGC 5408 X-1 during a flaring phase and from the break frequency and slopes either side of the break suggest a mass $\sim 100 M_{\odot}$. Finally, Goad et al. (2006) used the lack of variability power in a deep, high signal-to-noise *XMM-Newton* observation of Ho II X-1 to suggest an upper limit on its black hole mass of $100 M_{\odot}$. However, the calculation of PSDs is not always practical for ULXs given that as a class they do not tend to show much short-timescale variability. For example, Swartz et al. (2004) note short-timescale variability is detected in only 5 - 15 per cent of a large number of *Chandra* archival observations of ULXs, and Feng & Kaaret (2005) only find 3 out of 28 *XMM-Newton* ULX observations in their sample show detectable noise power in a PSD analysis.

The short-timescale variability that is present in the minority of ULXs might offer further clues as to their nature. In particular, the detection of periodicity could provide a view of the orbital characteristics of the binary system underlying the ULX. Perhaps the

most dramatic form this periodicity could take is eclipsing of the X-ray emission by the secondary star; interestingly, this could also be an indicator of the black hole mass, with stellar-mass black holes far more likely to show eclipses than IMBHs (Pooley & Rappaport 2005). However, known eclipsing ULXs remain rare – David et al. (2005) report a candidate in NGC 3379 with a 8-10 hr period, and a second candidate with a 7.5-hr period has long been known in the Circinus galaxy (Bauer et al. 2001) (though this latter object may instead be a foreground AM Her system; Weisskopf et al. 2004). Other reports of periods mainly rely on apparent periodic flux maxima in the light curves of the ULXs (for example Liu et al. 2002; Kaaret, Simet & Lang 2006a), though these detections are often based on very limited data (coverage of 2 - 4 times the suggested period only). The ambiguities in interpreting such data is highlighted by the case of M74 X-1 (CXOU J013651.1+154547), which was observed to undergo strong, relatively regular flaring behaviour during *Chandra* and *XMM-Newton* observations in 2001/2002. Liu et al. (2005) interpret this as quasi-periodic behaviour, and from this and the X-ray spectrum suggest a mass of $\sim (2 - 20) \times 10^3 M_{\odot}$, whereas Krauss et al. (2005) note that the behaviour resembles Galactic microquasars and suggest that the flaring could be related to a relativistic jet aligned with our line-of-sight.

The general lack of short-timescale variability exhibited by ULXs is to some degree extended to longer timescales by their persistent brightness. Indeed, many bright ULXs first observed by *Einstein* and subsequently re-observed by the following missions have remained active for more than 20 years with only modest flux variations between epochs (factors < 4 over ~ 20 years, e.g. Roberts et al. 2004). Such persistence is reminiscent of Galactic high-mass X-ray binaries with black hole primaries. Interestingly, Kalogera et al. (2004) predict that accretion from massive stars onto both stellar-mass black holes and IMBHs will appear reasonably persistent, with the key diagnostic being that IMBH systems will show transient behaviour on timescales of tens of years¹ No such complete turn-off has been seen so far from a famous ULX. Indeed, the majority of well-studied transient ULXs to date are likely to be similar in nature to known Galactic sources (Ghosh et al. 2006a; Mukai et al. 2005; Bauer & Pietsch 2005), though the spectrally hard, very luminous ULX close to the centre of NGC 3628 stands out as an IMBH candidate that has shown possible transient behaviour (Strickland et al. 2001).

A final temporal diagnostic is the spectral behaviour of ULXs, particularly by comparison to the behaviour of Galactic black hole X-ray binaries. *ASCA* observations of the ULXs in IC 342 identified spectra that apparently transited between low/hard (power-law dominated) and high/soft (accretion disc dominated) states in observations separated by 7 years (Kubota et al. 2001), which is similar to the most common behaviour in Galactic systems. However, many subsequent studies have highlighted ULXs that appear to show a contrary behaviour, in that they spectrally harden as their flux increases (e.g. Fabbiano et al. 2003; Dewangan et al. 2004). Fabbiano et al. (2003) note that this may indicate that ULXs are in a particularly high accretion rate state, though Jenkins et al. (2004) caution that the apparent difference may in part be due to the choice of X-ray colour bands used to define the hardness ratios.

Here, we present the results of a 2-month *Chandra* monitoring campaign on NGC 5204 X-1, that probes the variability diag-

¹ In Kalogera et al., the behavioural differences are anticipated to be between IMBHs of mass $> 50 M_{\odot}$ and less massive black holes, for accretion from fairly massive ($> 7 M_{\odot}$) young secondary stars.

nostics of this ULX on timescales from seconds to weeks. NGC 5204 X-1 is one of the brightest nearby ULXs with historical observed fluxes in the range $\sim 0.7 - 2 \times 10^{-12}$ erg cm $^{-2}$ s $^{-1}$ (0.5 – 8 keV), converting to luminosities of the order $2 - 6 \times 10^{39}$ erg s $^{-1}$ for a distance of $d = 4.8$ Mpc (Roberts et al. 2004). It is most notable for possessing stellar optical counterparts identified from its accurate *Chandra* position (Roberts et al. 2001; Goad et al. 2002), one of which was subsequently identified as a B0 Ib supergiant and suggested to be the actual counterpart due to UV spectral peculiarities consistent with some Galactic X-ray binaries (Liu, Bregman & Seitzer 2004). Initial short *Chandra* observations were hampered by low-level pile-up, but did reveal a steep power-law X-ray spectrum (Roberts et al. 2001, 2004). Subsequent *XMM-Newton* observations then revealed a spectral soft excess that might be interpreted as evidence of an IMBH accretion disc, though other spectral models not requiring the presence of an IMBH also fitted well to the data (Roberts et al. 2005; SRW06). In this paper we return to the issue of the nature of this ULX, as constrained by our X-ray monitoring campaign.

2 THE MONITORING CAMPAIGN

Previous observations of NGC 5204 X-1 have indicated that its flux varies by factors of ~ 3 over a baseline of years, but that little or no measurable variability was seen over timescales of minutes to a few hours (e.g. Roberts et al. 2004). Hence this monitoring campaign was designed to provide an indication of whether this ULX varies on timescales intermediate to those already probed, i.e. timescales of days to weeks. The *Chandra* X-ray observatory is the best choice for such a programme primarily due to its scheduling flexibility, combined with the spectral imaging capabilities of ACIS-S. The variability was investigated by a sequence of 11 observations spanning a period of two months (Table 1). An initial moderately-deep (50-ks) observation began the sequence, providing information on variability over the course of a ~ 14 hour interval. This was followed by a sequence of five short (5-ks) follow-up observations spaced at ~ 3 day intervals, to investigate variability over the course of days, then a further five (5-ks) observations spaced at ~ 10 day intervals to look at the variability on timescales of weeks. We summarise the observation details in Table 1, showing the exact start times and live-time corrected exposures. We also show an estimate of the mean *Chandra* ACIS-S count rate from NGC 5204 X-1 for each observation, which clearly demonstrates that the source flux is indeed varying over the day-to-week timescales examined.

A second aim of this programme was to characterise any spectral variability over the timescales probed. However, as Roberts et al. (2004) demonstrated, even employing the ACIS-S $\frac{1}{8}$ subarray mode in an attempt to mitigate pile-up was not fully successful for previous *Chandra* ACIS-S observations of NGC 5204 X-1. When the ULX was located on-axis, and was at its higher flux state (> 0.4 count s $^{-1}$), detectable pile-up effects were still evident in its X-ray spectrum. We therefore configured each observation such that NGC 5204 X-1 was located a distance of 4 arcminutes off-axis, displaced along the ACIS-S3 chip such that it remained in the middle of the spatial region covered by the $\frac{1}{8}$ subarray (i.e. an offset of $\Delta Y = -4$ arcmin in detector coordinates). The degradation of the *Chandra* point spread function at 4 arcminutes off-axis results in a 50% encircled energy radius of ~ 1.5 arcseconds, which compares to ~ 0.5 arcseconds on-axis. This is sufficient to ensure that any remaining pile-up is mitigated to manageable levels ($< 4\%$).

Table 1. Details of the *Chandra* observations.

Sequence number	Date and start time (yyyy-mm-dd@hh:mm:ss)	Exposure (s)	Count rate (count s $^{-1}$)
600307	2003-08-06@05:58:27	46227	0.20
600308	2003-08-09@09:36:20	4737	0.11
600309	2003-08-11@19:10:34	4500	0.13
600310	2003-08-14@16:35:34	4562	0.47
600311	2003-08-17@07:49:47	4635	0.45
600312	2003-08-19@23:28:06	5149	0.11
600313	2003-08-27@17:18:30	5143	0.11
600314	2003-09-05@16:11:45	4841	0.28
600315	2003-09-14@11:41:35	4877	0.46
600316	2003-09-23@09:33:01	5207	0.25
600317	2003-10-03@23:31:14	4896	0.41

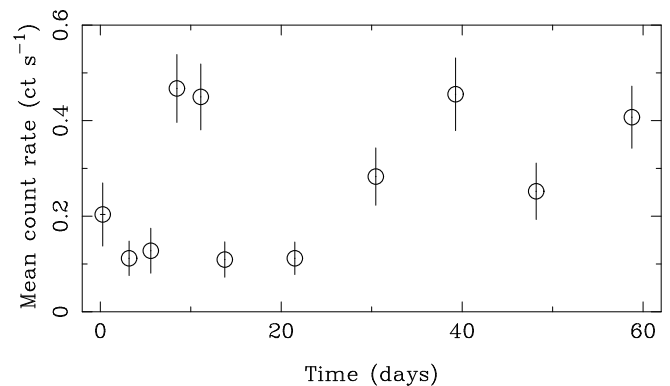


Figure 1. Full light curve for the monitoring campaign. We show the mean 0.5 – 8 keV band count rate per observation, and use the standard deviation on this count rate to represent the intrinsic variability per epoch.

The resulting data were reduced using standard tools within the CIAO 3.0 software suite, and version 2.23 of the *Chandra* Calibration Database. Pulse invariant spectra were extracted for each observation using the tool DMEXTRACT and response matrices and ancillary response functions (ARFs) were computed. Due to the build-up of the contaminant layer on the ACIS optical blocking filter, the ARFs were corrected using Alexey Vikhlinin’s tool CORRARF, now incorporated as a standard part of the CIAO spectral extraction.

In order to assess the validity of these products in light of calibration improvements made publicly available since our initial reduction, we reprocessed data from the 50-ks observation using CIAO 3.3 and the calibration database (CALDB) 3.2.1, and extracted new spectra. Minor differences in the response functions were found, primarily below 0.5 keV, with the functions being equivalent above 1 keV. Given that the impact to data in the 0.5–1 keV range was minimal, we elected not to reprocess the data presented herein.

3 TEMPORAL VARIABILITY

We present the 2-month monitoring light curve of NGC 5204 X-1 in Figure 1. The mean observed count rate of the ULX clearly varies by as much as factors of ~ 5 (in the 0.5 – 8 keV *Chandra* bandpass) between the observations, and the variations are statistically highly significant (a χ^2 fit against the hypothesis of a constant count rate, set to the mean count rate for the eleven observa-

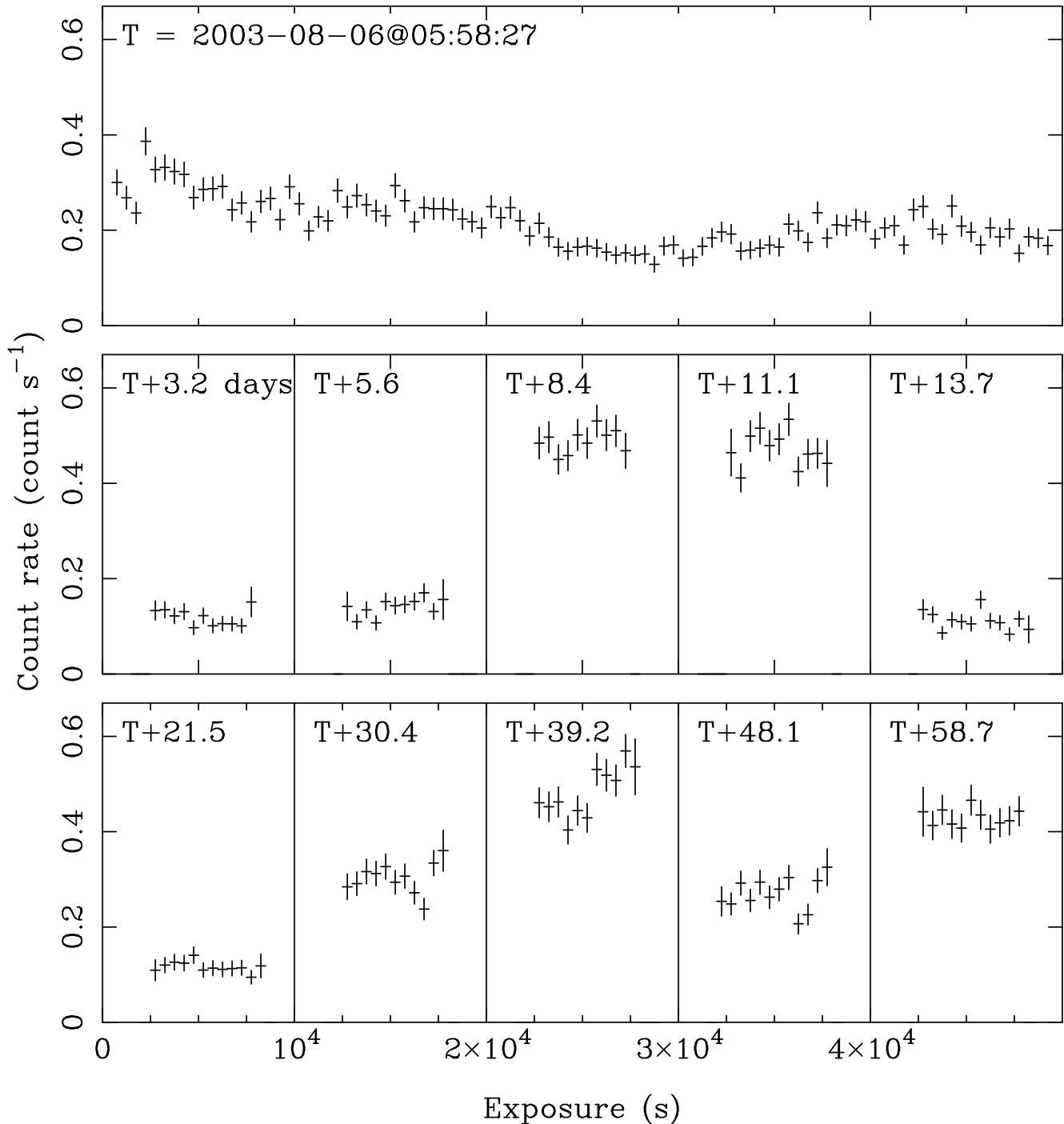


Figure 2. The full light curve for the monitoring programme of NGC 5204 X-1, binned to 500 s resolution.

tions, gives a statistic of 95.5 for 10 degrees of freedom). Most interestingly, the source appears to have upper and lower thresholds that are not exceeded (albeit within the very limited sampling of this programme), confining the flux measurements to between ~ 0.1 and 0.5 count s^{-1} . In fact, these limits do not appear to have been exceeded throughout the historical record of observations of this source (cf. Roberts et al. 2004, Figure 6(f), where the extreme flux points are both from *Chandra* ACIS-S data, and correspond to count rates of ~ 0.41 and $\sim 0.16 \text{ count s}^{-1}$).

The light curve, though sparsely sampled, does not betray any

obvious periodic signature. This is particularly interesting for NGC 5204 X-1 where a positive identification of the secondary star in this system as a B0 Ib supergiant, and the assumption of Roche lobe overflow, leads to firm predictions of the orbital period of between $\sim 200 - 300$ hours for a wide range of primary black hole masses ($3 - 1000 M_{\odot}$; Liu et al. 2004). Our ~ 59 day baseline covers between 5 and 7 cycles of these possible orbital periods. We have searched for possible hidden periodic signals by deriving a Lomb-Scargle periodogram from the data. A visual inspection of the periodogram suggested possible periodic signals of ~ 10 and

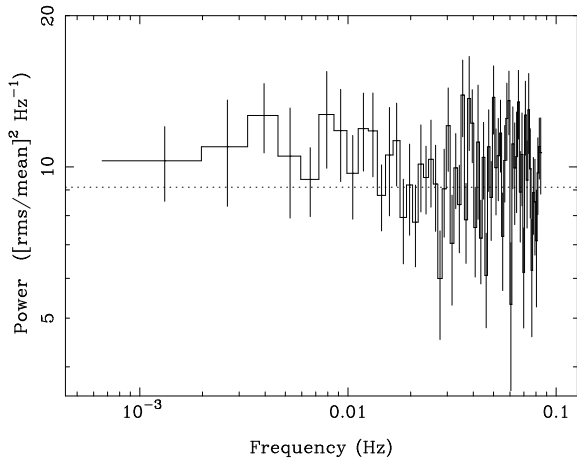


Figure 3. The power spectral density of the 50-ks exposure. It was calculated by dividing the light curve into 64 segments of 128 points, and the FFT of each segment was computed and averaged to produce the plot. Errors were computed in the standard fashion from the dispersion of the 64 data points within each frequency bin. The PSD was normalised using the $(\text{rms}/\text{mean})^2$ convention defined by van der Klis (1997). Using this normalisation the expected Poisson noise level (shown with the dotted line) is $2/\mu$ (where μ is the mean count rate).

16 days (i.e. ~ 240 and 384 hours). We further investigated these signals by fitting a model composed of a sinusoidal function plus a constant component to the lightcurve, and did indeed find a best-fit to the data at ~ 10 days. However this fit produced a χ^2 statistic of 27.4 for 7 degrees of freedom (dof), which has a null hypothesis probability of only 3×10^{-4} , hence there is very little chance of this being a true periodic signal. The fit for a 16-day period was even worse ($\chi^2/\text{dof} = 39.5/7$). We conclude that there is little or no evidence for periodicity in the X-ray emission from this dataset.

In Figure 2 we show the eleven individual lightcurves at 500-s resolution, plotted on a convenient scale for direct comparison. An inspection by eye reveals that as one looks at shorter timescales the amplitude of variability in this source is apparently less. That is to say, during the 50-ks observation clear trends are visible, starting with a diminution in count rate from $\sim 0.3 \text{ count s}^{-1}$ in the first 5 ks to $\sim 0.15 \text{ count s}^{-1}$ after ~ 30 ks, followed by a slight brightening to $\sim 0.2 \text{ count s}^{-1}$ for the remainder of the observation. However, trends and/or large amplitude variations are less visible within the shorter follow-up observations. We performed standard statistical tests to check for significant intrinsic variability (i.e. a χ^2 test against the hypothesis of a constant count rate for data binned to 100 or 200 second resolution, and a Kolmogorov-Smirnov test at the full 0.74104 s temporal resolution of the ACIS-S3 $\frac{1}{8}$ subarray), and found that the only observation showing highly significant variability was indeed the 50-ks look (sequence number 600307, $\gg 10\sigma$ significance in both tests). Only one other observation showed variability at $> 3\sigma$ significance, namely 600315 (at T + 39.2 days) that was significant at the $\sim 4\sigma$ level according to the K-S test (though, in contrast, the χ^2 test showed a significance $< 2\sigma$ for this observation). There was no strong evidence of any short-term variability intrinsic to the data in any other observation.

The increase in intrinsic variability over longer timescales is typical of a source showing a red noise dominated fluctuation power spectral density (PSD). We have checked this by calculating the PSD from the longest (50-ks) observation, which we show in Figure 3. The PSD is clearly poisson-noise dominated above 0.02 Hz, though some excess power may be evident below this fre-

Table 2. Mean hardness ratio values within flux-limited ranges.

Range	Count rates (ct s^{-1})	HR1	HR2
Faint	< 0.2	-0.23 ± 0.01	-0.71 ± 0.02
Medium	$0.2 - 0.4$	-0.11 ± 0.01	-0.55 ± 0.01
Bright	> 0.4	-0.03 ± 0.01	-0.54 ± 0.01

quency (i.e. on timescales > 100 s), consistent with a red noise source spectrum. However, the data for this potential red noise component are so poor that we are unable to constrain any possible measurement of the power-law slope characterising this component at the 90% level. We note that as the variability increases to factors up to ~ 5 over time scales of ~ 3 days the putative red noise spectrum should continue down to, and become more apparent at, frequencies longer than those covered in the 50-ks observation.

We have also investigated whether the broad spectral form of the ULX alters during our monitoring campaign by examining spectral hardness ratios calculated from the data. We binned the data into 1-ks intervals and segregated it into three energy bands, a 0.3 – 1 keV soft (*S*) band, a 1 – 2 keV medium (*M*) band, and a 2 – 8 keV hard (*H*) band. We then calculated our hardness ratios as $\text{HR1} = (M - S)/(M + S)$ and $\text{HR2} = (H - M)/(H + M)$, with errors on the hardness ratios calculated as per Ciliegi et al. (1997).

An initial examination of the energy-segregated lightcurves suggested that there may be spectral variations as the total flux of the source changes. We investigated this further by comparing the hardness ratios to the total count rate of NGC 5204 X-1, which we show here in Fig. 4. There does indeed appear to be a trend over the course of the campaign, with the ULX appearing to be relatively soft in its lowest flux states, and to harden significantly as its flux increases. This appears to be the case for both hardness ratios. Remarkably this behaviour appears contrary to the classic low/hard to high/soft state transitions commonly seen in Galactic black hole binaries though, as we noted earlier, similar behaviour has been observed before in other ULXs. We quantify this relationship in Table 2, where we split the data into three broad bins based on the total count rate, and calculate a weighted mean of the hardness ratio values within that count rate range. In the softer of the two ratios, HR1, we see that the average source spectrum hardens over all three bins. However, the average HR2 value is consistent between the two brighter count rate bins, and only significantly softer in the faintest bin. We investigate the nature of these spectral variations, and their dependence on the brightness of NGC 5204 X-1, in the next section.

4 SPECTRAL VARIABILITY

Spectral data were extracted in an elliptical aperture, with major and minor axes of ~ 7.8 and ~ 4.3 arcseconds respectively, designed to encompass the full *Chandra* point spread function for X-ray photons from NGC 5204 X-1 at ~ 4 arcminutes off-axis. Background data were extracted in an elliptical annulus, centered on the ULX and with inner and outer axial dimensions of 1 and 4 times the source extraction ellipse axes respectively. The spectral data were grouped to a minimum of 20 counts per bin, to ensure χ^2 statistics are valid. Spectral fitting was then performed over the 0.5

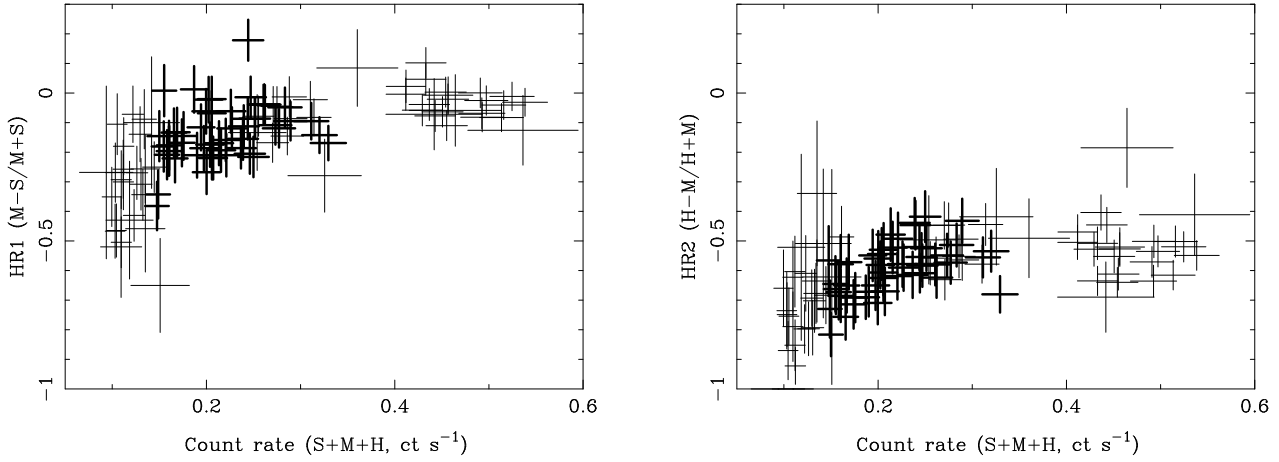


Figure 4. Variations in the spectral hardness ratios of NGC 5204 X-1 with overall count rate. The hardness ratios are calculated in 1 ks intervals, as per the method discussed in the text. We plot data from the deep (50 ks) observations as thick crosses, with the data from the ten shorter follow-up observations as thin crosses.

– 10 keV range², using XSPEC v.11.3.0. The errors quoted throughout the analysis are 90% errors for one interesting parameter unless otherwise stated.

4.1 The X-ray spectrum from the 50-ks observation

We began our spectral analysis by examining the full spectral data set for NGC 5204 X-1 from the initial 50-ks observation. In this and the subsequent analysis we fitted two absorption columns: a Galactic foreground absorber set to the line-of-sight in the direction of NGC 5204 (1.5×10^{20} atom cm^{-2} ; Stark et al. 1992), and an additional absorption column presumably located along the line-of-sight in NGC 5204, or in the local vicinity of the ULX. In both cases we used the interstellar abundances and absorption cross-sections tabulated by Wilms, Allen & McCray (2000) (the TBABS model in XSPEC).

Initial fits to the data were attempted using absorbed, single-component spectral models. However, despite trying a wide range of simple models (e.g. blackbody; thermal bremsstrahlung; multi-colour disc blackbody; MEKAL optically-thin thermal plasma) no good fit to the data was found. The best-fitting simple model was an absorbed power-law continuum, as found in previous observations of NGC 5204 X-1 (Roberts et al. 2001, 2004, 2005), in this case with $N_H = (1.3 \pm 0.2) \times 10^{21}$ cm^{-2} and $\Gamma = 2.83 \pm 0.08$. However this was still rejected at high significance (χ^2/dof of 212.3/141, i.e. a rejection probability of $P_{rej} = 99.99\%$).³ We show the power-law fit and residuals in Fig. 5. As with previous observations, the overall continuum shape of this ULX is soft. However, this spectrum is remarkable in that it shows a large residual feature at $\sim 0.8 - 1$ keV, with further possible residuals evident at both lower and higher energies.

As we cannot achieve good fits using single component spectral models, we turned to two-component models. Specifically, we tried the empirical models discussed at length in Roberts et al. (2005), utilised in fitting the *XMM-Newton* spectrum of this source.

² Data below 0.5 keV were not considered in this analysis due to calibration uncertainties in this regime. In addition, although we quote 10 keV as the upper limit, in practise we have only one data bin above 6 keV.

³ We consider spectral fits to be formally acceptable if their rejection probability is $< 95\%$.

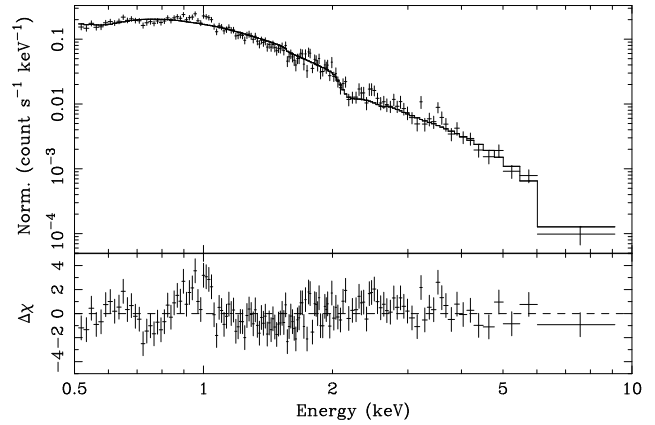


Figure 5. Power-law continuum fit to the spectrum of the 50 ks observation. The upper panel shows the data and best fitting power-law model (see text for details), and the lower panel shows the $\Delta\chi$ residuals to this model.

These were the standard empirical description of a black hole X-ray binary spectrum, a soft multicolour disc blackbody plus a harder power-law continuum, and the non-standard inversion of this spectrum where the power-law continuum dominates at soft energies. We note that the *XMM-Newton* data showed ambiguity between these two models, i.e. it did not indicate a strong preference for one or the other. We again find that our data does not strongly distinguish between these two models for NGC 5204 X-1, with best fitting parameters of inner accretion disc temperature $kT_{in} \sim 0.18$ keV and power-law photon index $\Gamma \sim 2.7$ for the standard model fit, and $kT_{in} \sim 1.2$ keV, $\Gamma \sim 3.9$ for the non-standard fit. However, unlike the *XMM-Newton* observation, neither model provides a good description of the data in this case, with both rejected at 99.96% significance.

Instead, statistically-acceptable fits were found using two-component models in which the soft component was modelled by a MEKAL thermal plasma. Good fits (rejection probability $P_{rej} < 80\%$) were found using either a power-law continuum or a multi-colour disc blackbody as the hard component. We detail these fits as Models (1) and (2) in Table 3. When a power-law continuum describes the harder emission the MEKAL temperature is ~ 0.96 keV, and its abundance is approaching solar, whereas when the multi-

Table 3. Spectral modelling of the 50 ks *Chandra* observation of NGC 5204 X-1.

Model component ^a		Spectral models ^a				
		(1) MEKAL + PO	(2) MEKAL + DISKBB	(3) BB + PO + GAUSS	(4) BB + DISKBB + GAUSS	(5) COMPTT + GAUSS
TBABS	N_H ^b	< 1.2	< 0.05	$0.98^{+0.68}_{-0.58}$	< 0.19	< 0.45
MEKAL	kT ^c	0.96 ± 0.09	$0.84^{+0.05}_{-0.06}$	-	-	-
	Z ^d	$0.62^{+2.92}_{-0.52}$	0.04 ± 0.01	-	-	-
PO	Γ ^e	$2.55^{+0.12}_{-0.40}$	-	$2.92^{+0.23}_{-0.17}$	-	-
DISKBB	kT_{in} ^f	-	$1.43^{+0.25}_{-0.18}$	-	0.92 ± 0.06	-
	A_{dbb} ^g	-	$(4.4^{+3.7}_{-2.2}) \times 10^{-3}$	-	$(4.6^{+1.6}_{-1.2}) \times 10^{-2}$	-
BB	kT ^h	-	-	$0.67^{+0.12}_{-0.13}$	0.17 ± 0.01	-
GAUSS	E ⁱ	-	-	0.96 ± 0.02	0.97 ± 0.02	0.96 ± 0.02
	σ ^j	-	-	$0.08^{+0.02}_{-0.03}$	0.06 ± 0.03	0.07 ± 0.03
COMPTT	EqW ^k	-	-	85^{+22}_{-40}	51^{+23}_{-17}	75^{+33}_{-21}
	T_0 ^l	-	-	-	-	$0.11^{+0.01}_{-0.04}$
	kT_e ^m	-	-	-	-	$1.41^{+0.37}_{-0.35}$
	τ ⁿ	-	-	-	-	$6.7^{+1.6}_{-1.3}$
χ^2/dof		150.6/138	151.6/138	140.5/136	145.7/136	139.1/136

Notes: ^a In XSPEC syntax. All models are subject to an additional, fixed Galactic column of $1.5 \times 10^{20} \text{ cm}^{-2}$. ^b Absorbing column external to our own Galaxy, in units of 10^{21} cm^{-2} . ^c Plasma temperature (keV). ^d Plasma metallicity (solar units). ^e Power-law photon index. ^f Inner-disc temperature (keV). ^g Model normalisation. ^h Black-body temperature (keV). ⁱ Line centroid energy (keV). ^j Line width (keV). ^k Equivalent width of line (eV). ^l Seed photon temperature for corona (keV). ^m Comptonising corona electron temperature (keV). ⁿ Optical depth of corona.

colour disc blackbody models the hard component we require a cooler (~ 0.84 keV), low metallicity MEKAL.

In order to investigate whether any specific features were driving the MEKAL fits to the soft part of the spectrum, we proceeded to fit the spectral data with a combination of smooth continuum models and emission lines. As we were able to fit the hard component with either a power-law or a multi-colour disc blackbody in Models (1) & (2), we therefore attempted two continuum fits, one with each as the hard component. We chose to use a classic blackbody as the soft component. This results in two empirical models with possibly quite different physical origins, i.e. an accretion disc plus hot corona model (blackbody + power-law continuum), and an accretion disc plus a soft excess model (in which the soft excess is modelled by the blackbody). The use of both models resulted in good fits to the data above 1 keV, but left large residuals at lower energies as expected. In both cases we were able to fit these residuals, and hence provide an acceptable fit to the full dataset, using a single broad gaussian line at an energy of ~ 0.96 keV (cf. Models (3) & (4) of Table 3). However, neither underlying continuum model appears to support the presence of a cool ($\sim 0.1 - 0.3$ keV) accretion disc in this ULX, that one would expect if an IMBH were present.

There has been some recent speculation that ULXs may form preferentially in low-metallicity environments, as these potentially allow the formation of large black holes (cf. Soria et al. 2005 and references therein). Evidence in support of this has recently emerged in a deep *XMM-Newton* observation of the Ho II ULX (Goad et al. 2006), where an apparent excess of counts above 0.5 keV in the RGS spectrum of this ULX was best explained by reducing the metallicity of the absorbing material to ~ 0.6 of the solar values. If we allow the metallicity of the second of our absorption components to vary (by using the TBVARABS model, with all abundances constrained to the same value as a first approximation) we find that a sub-solar abundance does provide a marginal improvement to the fit for Model (3), though as Model (4) includes little or no extra absorption above the Galactic foreground column

it is insensitive to this test. The actual improvement for Model (3) is $\Delta\chi^2 = 5.1$ for one extra degree of freedom, which is marginally significant (at the $\sim 2\sigma$ level) according to the F-test. The parameterisation of Model (3) is essentially unchanged, apart from a substantially higher column of $4.5^{+2.6}_{-2.3} \times 10^{21} \text{ cm}^{-2}$, and a limit of < 0.26 times solar abundance for the metallicity of the absorbing medium.

Finally, we attempted to fit a physical accretion disc plus corona model to the data, as one might expect to see for an accreting black hole. As per the work of Goad et al. (2006) on Ho II X-1, we used a DISKPN + COMPTT model (subject to the same solar-abundance absorption components as the empirical models), with the two components linked by using the temperature of the disc to provide the input temperature of the seed photons for the corona. This model did not provide a statistically-acceptable fit to the data, with the best fit having $\chi^2/\text{dof} = 194/138$, though it did have the interesting characteristic of being totally dominated by the coronal component. An inspection of the residuals to this fit showed that the feature at ~ 1 keV was not adequately explained by this model; we therefore again added a Gaussian line. Similarly to the empirical models, this provided a statistically-acceptable fit to the data, which we show as Model (5) of Table 3. In fact, it provides the statistically best fit to the data, albeit by a small margin.⁴ We show the data and Model (5) fit in Fig. 6. Even after the addition of the line - which shows very similar properties to the line derived from the empirical fits - the contribution of the disc component is negligible ($\ll 1\%$ of the 0.5 – 8 keV flux), so we only show the parameterisation of the coronal component in the Table. This component shows the same remarkable characteristics as the corona in Ho II X-1, i.e. it is cool ($kT_e \sim 1.4$ keV), optically-thick ($\tau \sim 7$)⁵

⁴ This is not simply due to allowing more degrees of freedom to vary in the Comptonisation model than are present in empirical models - in fact, this fit has the same number of degrees of freedom as models (3) and (4).

⁵ The COMPTT model is not fully self-consistent, and may underestimate the actual depth of the corona. For example, SRW06 model the Ho II X-1

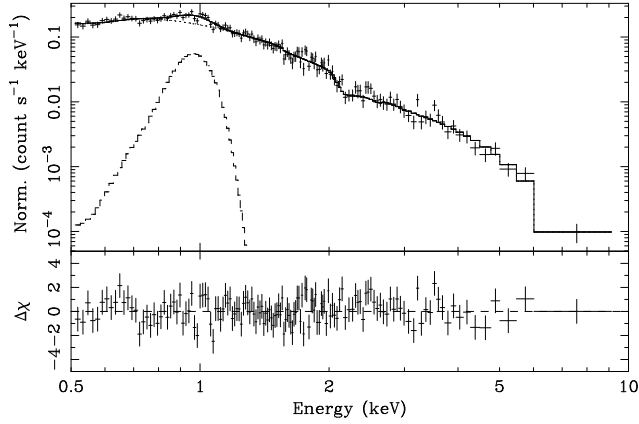


Figure 6. Model (5) fitted to the spectrum of the 50 ks observation. The upper panel shows the data and best fitted model, with the contribution of the gaussian line and the optically-thick corona highlighted by dashed and dotted lines respectively (as can be seen, the corona effectively models the full continuum other than in the 0.8 - 1.1 keV regime). The lower panel shows the $\Delta\chi$ residuals to this model.

and seeded by photons originating in a cool (~ 0.1 keV) disc. Interestingly, this is supportive of other recent work, most notably a sample of 13 bright ULXs observed with *XMM-Newton* (SRW06), that shows that it is plausible that the X-ray spectra of a large proportion of ULXs are well described by an optically-thick coronal component seeded by a cool disc. We note that by fixing $kT_e = 50$ keV and re-fitting, one can get a statistically-acceptable solution with an optically-thin corona ($\tau \sim 0.2$, $\chi^2/\text{dof} = 150.6/137$), though this does require the disc temperature to reduce further to ~ 20 eV. However, an F-test shows that the improvement offered over this by the optically-thick solution is significant at the $\sim 3\sigma$ level. We therefore view an optically-thick solution as far more realistic.

The spectral modelling results in a typical observed 0.5 – 8 keV flux of $\sim 9.8 \times 10^{-13}$ erg cm $^{-2}$ s $^{-1}$ (with only a few per cent disagreement between the models in Table 3), from which we can derive an average luminosity of $\sim 2.7 \times 10^{39}$ erg s $^{-1}$ over the duration of the observation.

4.2 Spectral variability within the 50 ks observation

As Fig. 4 shows, the factor ~ 2 variation in flux during the observation is accompanied by some spectral variation. We have investigated whether we can quantify this variation through spectral fitting in the following manner. We first selected and extracted spectral data from three 10-ks segments within the 50-ks observation, these being the 5 – 15, 25 – 35 and 40 – 50 ks windows. Roughly speaking, these correspond to relatively stable high (> 0.2 count s $^{-1}$), low (< 0.2 count s $^{-1}$) and medium (~ 0.2 count s $^{-1}$) flux states during the observation (cf. Fig. 2; we refer to each segment by these respective titles hereafter). The relative differences in these spectra are demonstrated in Fig. 7, where we plot the $\Delta\chi$ residuals for each time segment spectrum against the best fitting model to the whole observation (Model (5), i.e. the optically-thick coronal model).

In order to study these spectral differences, we loaded all three datasets into XSPEC simultaneously. The varying components of

corona using the more physical EQPAIR model, and find an optical depth a factor 2 deeper than Goad et al.’s COMPTT modelling.

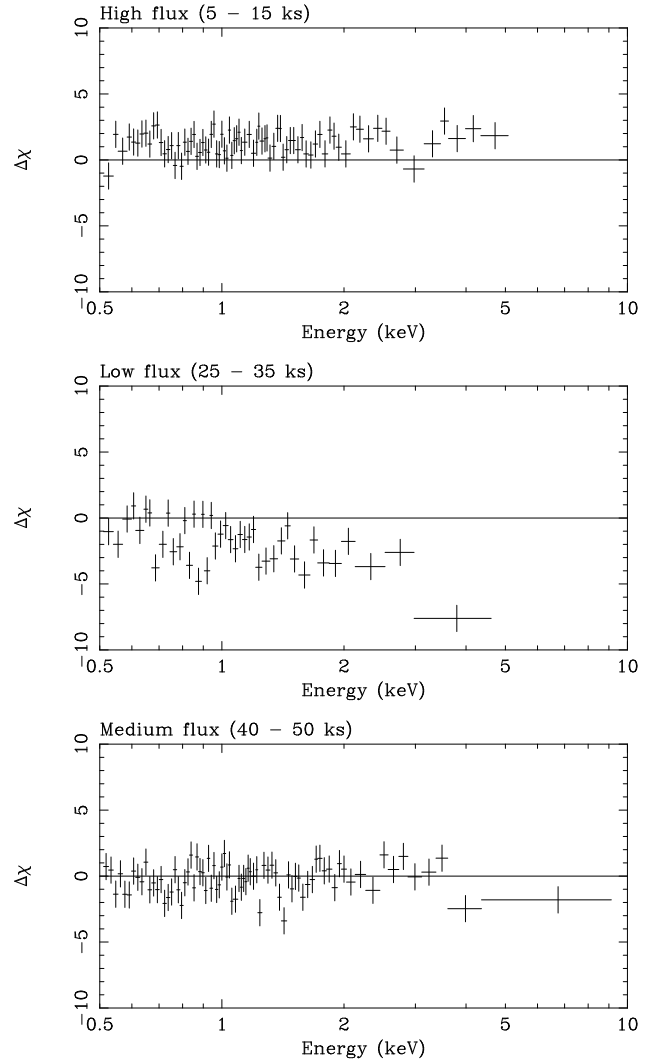


Figure 7. The spectral variability of NGC 5204 X-1 during the 50 ks observation. We use the three segments described in the text, and plot the $\Delta\chi$ residuals against the Model (5) fit, i.e. the best-fitting description of the spectrum of the whole observation. The three panels are shown on the same scale for direct comparison.

each spectral model were identified by first freezing all the model components, and then thawing the parameters one-by-one, untying their values across the three datasets, and re-fitting. Those parameters offering the largest reduction in the overall χ^2 value for the simultaneous fit were judged to be the most important in explaining the spectral variation of the ULX.

As Fig. 7 shows, a comparison of the spectral segments to the model best-fitting the whole spectrum demonstrates the presence of considerable residuals. Indeed, when loaded into XSPEC this model proved a very poor simultaneous fit to the three data segments, with a χ^2/dof value of 572/200. The majority of spectral variability appears to originate above 1 keV, particularly in the case of the “low” segment spectrum, where considerable additional curvature is present. We find that this spectral variability can be very simply and adequately modelled by a variation in the temperature of the coronal component, which provides a statistically-acceptable fit to the data ($\chi^2/\text{dof} = 226.7/197$, i.e. $P_{rej} \approx 93\%$). A striking feature of this fit is that it appears that the temperature of the coronal component falls and rises in line with the flux of the ULX, that is

Table 4. Varying spectral parameters within the 50-ks observation.

Segment (ks)	kT_e^a	τ^b	f_X^c	L_X^d
5 – 15	1.74 ± 0.09	6.2 ± 0.4	$13.2^{+0.3}_{-0.4}$	3.7 ± 0.1
25 – 35	1.10 ± 0.09	$6.9^{+0.8}_{-0.7}$	6.2 ± 0.2	1.8 ± 0.1
40 – 50	1.29 ± 0.07	7.1 ± 0.5	$9.0^{+0.3}_{-0.2}$	2.6 ± 0.1

Notes: ^a Temperature of corona in keV. ^b Optical depth of corona.

^c Observed 0.5 – 8 keV flux, in units of $\times 10^{-13}$ erg cm⁻² s⁻¹.

^d Intrinsic 0.5 – 8 keV luminosity, in units of $\times 10^{39}$ erg s⁻¹.

to say it is at its coolest when the flux is lowest, and vice versa (see Table 4). A slight additional improvement to the fit is offered by thawing and untying the optical depth of the corona, though as it offers a mere $\Delta\chi^2 = 6.9$ improvement for three additional degrees of freedom it is not statistically robust. However, we still tabulate the best-fitted values of τ in Table 4 (alongside the best-fitted coronal temperatures and fluxes for each segment) as we take the view that changes in the optical depth are at least a plausible occurrence as the coronal temperature varies. Furthermore, we note that freeing either the temperature of the seed photons, or the normalisation of the coronal model, does not provide any improvement to the fit. Finally, in this model there is no necessity for the flux, central line energy or line width of the Gaussian component at 1 keV to vary at all during the observation.

4.3 Spectral variability throughout the programme

As Fig. 4 indicates, the spectrum of NGC 5204 X-1 seems to vary in a consistent manner as the count rate varies across the entire dataset, including the series of follow-up observations. We therefore hypothesize that the observed X-ray variability during the entire monitoring campaign can be explained by the optically-thick corona model (i.e. Model (5)), as proved adequate for the intra-observation variability during the 50-ks observation. Unfortunately, the data from the 5-ks snapshots are generally of insufficient quality to constrain the fits (particularly when the count rate is low). We therefore co-added spectra to produce reasonable quality data to work with. Specifically, we co-added spectra from observation sequence numbers 600308, 600309, 600312 and 600313, to provide a “faint” state spectrum, as all these observations had average count rates in the 0.11 – 0.13 count s⁻¹ regime. Similarly, we combined spectra from observation sequence numbers 600310, 600311, 600315 and 600317 (i.e. where average count rates were between 0.41 – 0.47 count s⁻¹), to provide a “bright” state spectrum. Again, we began by comparing the extracted spectra to the best fitted spectrum from the deep observation (Model (5)), and note that both co-added spectra showed considerable changes relative to this spectrum. We again demonstrate this by plotting the $\Delta\chi$ residuals of these datasets compared to Model (5) in Figure 8.

We find that the faint state spectrum is very adequately explained by the optically-thick corona model, with $\chi^2/\text{dof} = 67.8/69$. The majority of the variability can be modelled as a change in the coronal temperature, with additional marginally significant improvements (at the $\sim 95\%$ level according to the F-test) offered by changes in the optical depth of the corona and, for the first time, changes in the temperature of the photons seeding the corona (i.e. the accretion disc temperature). Interestingly, the 90% errors on the parameters do allow an optically-thin, hot corona solution in this case, but again only if the accretion disc temperature reduces further to ~ 20 eV. We note that the presence of the Gaus-

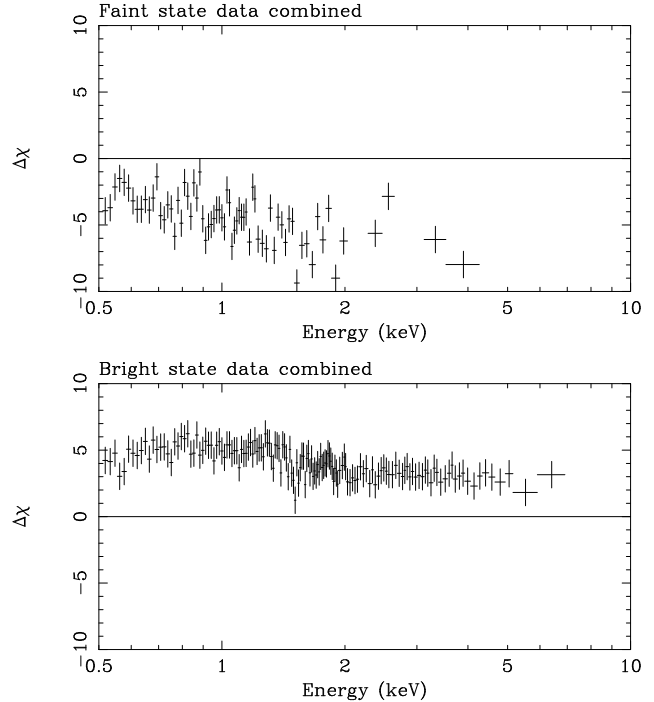


Figure 8. The spectral variability of NGC 5204 X-1 from the follow-up observations. As per Fig. 7, we plot the $\Delta\chi$ residuals against the Model (5) fit. The panels are shown on the same scale as the previous Fig. for direct comparison, though we note that this excludes two data points from the top panel in the 2 – 3 keV regime, that lie at $\Delta\chi \sim -15$.

sian line is required in this fit - indeed, setting its normalisation to zero degrades the goodness of the fit significantly ($\Delta\chi^2 = 50$).

The bright state cannot be as readily explained using Model (5). Thawing each of the coronal temperature, its optical depth and seed photon temperature in turn provides a significant improvement to the fit each time, though the resultant fit has $\chi^2/\text{dof} = 195/146$, i.e. it is rejected at the 99.6% confidence level. However, an inspection of the residuals reveals that just two isolated bins (at ~ 1.5 and ~ 5.5 keV) disagree strongly with the model, providing $\Delta\chi^2 \approx 18$ each to the fit. If they are removed, the fit becomes tenable ($\chi^2/\text{dof} = 159/146$, i.e. $P_{rej} < 80\%$). We therefore conclude that, assuming these two bins do not represent real spectral features⁶, the underlying spectral form is still adequately modelled by the optically-thick corona model.

We compare the spectral parameters from the bright and faint co-added spectra with the parameters from the 50-ks observation (derived whilst the Gaussian parameters and absorption remained frozen, as is the case for the co-added spectra) in Table 5. In

⁶ The deficit present in the ~ 5.5 keV bin can be modelled by an edge feature, at an energy of 5.1 ± 0.2 keV, with a depth of $0.9^{+0.6}_{-0.4}$ keV. This produces an improvement of $\Delta\chi^2 = 20.4$ for two extra degrees of freedom, and results in a fit that is only marginally rejected ($P_{rej} = 95.8\%$). However, an edge at this energy may be astrophysically implausible - the nearest edge is neutral Ti (~ 5 keV), or if it were to be an edge from neutral Fe it would require a redshift of ~ 0.3 . No such improvement is possible for the 1.5 keV bin, which is unlikely to be a real feature as its width is far narrower than the ACIS-S resolution at that energy. There are no known ACIS-S calibration issues at this energy, and an inspection of the individual contributory spectra indicates that this feature originates in the juxtaposition of less significant residual data points from two out of four spectra, indicating this feature may simply be an extreme statistical fluctuation.

Table 5. Varying accretion disc plus corona spectral parameters over the campaign, and for an earlier *XMM-Newton* observation.

Obs.	T_0^a	kT_e^b	τ^c	f_X^d	L_X^e
50-ks	0.11 ± 0.01	$1.41^{+0.13}_{-0.11}$	6.7 ± 0.4	$9.8^{+0.1}_{-0.2}$	$2.8^{+0.0}_{-0.1}$
Faint	$0.09^{+0.02}_{-0.08}$	$1.22^{+0.67}_{-0.28}$	$6.2^{+1.2}_{-5.2}$	$4.6^{+1.3}_{-0.8}$	$1.3^{+0.4}_{-0.2}$
Bright	0.14 ± 0.01	$2.29^{+0.14}_{-0.12}$	5.1 ± 0.2	23^{+11}_{-3}	$6.4^{+3.0}_{-0.8}$
<i>XMM</i>	$0.11^{+0.03}_{-0.02}$	$1.99^{+0.38}_{-0.24}$	$7.5^{+0.7}_{-0.8}$	14^{+2}_{-6}	$3.9^{+0.6}_{-1.7}$

Notes: ^a Temperature of photons seeding the corona (keV) ^b Temperature of corona in keV. ^c Optical depth of corona. ^d Observed 0.5 – 8 keV flux, in units of $\times 10^{-13}$ erg cm⁻² s⁻¹. ^e Intrinsic 0.5 – 8 keV luminosity, in units of $\times 10^{39}$ erg s⁻¹.

this comparison we see apparent differences in the temperature of the seed photons (i.e. the underlying accretion disc) between the epochs when the ULX is at different mean fluxes. As these flux changes only occur on timescales of days, it is interesting to note that this may indicate that the accretion disc temperature changes are occurring on the same timescale. It is certainly true that in the one instance we are sensitive to shorter timescale variations in the accretion disc temperature, i.e. in the 50-ks observation, we do not see such an effect. We note again that the temperatures - in this case of both the seed photons and the corona - appear to vary in line with the overall flux of the spectrum, with the system being hotter when it is brighter, though the optical depth appears to vary independently in this comparison.

Whilst this and the previous section have demonstrated that the spectral variability of NGC 5204 X-1 can readily be explained through changes in the dominant coronal component of Model (5), this was not the only spectral model capable of providing an acceptable fit to the full data from the 50-ks observation. By repeating the above analysis for the other spectral models in Table 3 we find that Models (1), (3) and (4) can all also adequately describe the spectral variations (we exclude Model (2) for reasons explained below in Section 5.2). We tabulate the variable parameters for these models in Table 6. In each case, the component responsible for the ~ 1 keV feature - a MEKAL in Model (1), or Gaussian line in Models (3) & (4) - remains invariant, whilst the other parameters are required to change to provide an acceptable fit to the data.⁷ In each case, the fitted parameter values again reflect the pattern of spectral hardening with increased luminosity.

4.4 A comparison with *XMM-Newton* data

As a final metric of the longer term spectral variations of NGC 5204 X-1 we have re-analysed data from an *XMM-Newton* observation of NGC 5204 X-1 taken 8 months before our monitoring programme commenced. This data set (Observation ID 0142270101) was taken on 2003 January 6, and provides 15.4/18.5 ks of live-time corrected exposure in the EPIC pn/MOS instruments respectively, with data quality comparable to the 50-ks *Chandra* observation. (We note that there were two further observations of NGC 5204 X-1 taken

⁷ In fitting the models, we allowed the power-law normalisations for Models (1) and (3), and the normalisation for the blackbody in Model (4), to vary. A variation in the normalisations for the components plausibly describing an accretion disc - the blackbody in Model (3), and the multi-colour disc blackbody in Model (4) - was not required, consistent with changes in the temperature of the inner-edge of the accretion disc.

in mid-2003, but both were subject to strong background flaring leaving little useful exposure for analysis.) The results of this observation have previously been discussed by Roberts et al. (2005) and SRW06. Here we use the *XMM-Newton* science analysis software (SAS) version 6.5.0 to re-extract the data from the original observation data files (ODFs) available in the *XMM-Newton* science archive, in order to take advantage of refinements in the calibration of the EPIC instruments. We then created 0.3 – 10 keV source spectra from this data, and fit them in XSPEC, in the manner described by Roberts et al. (2005).

The data were firstly fitted with Model (5) using the same methodology as in the previous sections, i.e. the best fitting parameters from the 50-ks *Chandra* observation were thawed one-by-one to assess whether variations from the parameter in question best explain the difference between data sets. In this case we were required not just to vary the three physical parameters used to describe the variations in the *Chandra* data (T_0 , kT_e and τ), but also the normalisations of the disc and coronal components, in order to achieve an acceptable fit. We show the best fit parameterisation of the *XMM-Newton* spectra using Model (5) in Table 5. The *XMM-Newton* data appears to follow the same flux - coronal temperature relationship as observed for the various *Chandra* data. Unlike the *Chandra* data, we were able to measure an appreciable contribution to the spectrum from an accretion disc component in the *XMM-Newton* data, likely due to the slightly softer response of EPIC compared to ACIS. However, this was small, amounting to only ~ 2.5 per cent of the observed flux in the 0.3 – 10 keV band, though as SRW06 found the disc contribution in empirical disc plus corona models rarely amounts to more than 10 per cent of the flux in this band for ULXs.

As in the previous section, we also fit the *XMM-Newton* data with Models (1), (3) and (4). The results are shown in Table 6. Again, we required that extra normalisations were thawed and re-fit in order to get statistically-acceptable fits, notably the normalisations for the disc components in Models (3) and (4). The parameterisation of the *XMM-Newton* fits emphasize that this spectrum appears different to the subsequent *Chandra* observations. Overall, they betray a harder spectrum, with both harder spectral parameters, and a general diminution of the flux in the softer component. For example, the flux in the MEKAL component in Model (1) is reduced to ~ 20 per cent of its value in the later *Chandra* observations (though, where present, the flux of the Gaussian feature is again not required to change in order to obtain a good fit). Hence it appears that in the eight months between the *XMM-Newton* observation and the *Chandra* monitoring the spectrum of NGC 5204 X-1 softened, in large part due to an increase in flux at low energies. Finally, we emphasize that these models are just a sub-set of those fitting this data, and refer the reader to Roberts et al. (2005) and SRW06 for more discussion.

5 DISCUSSION

5.1 On the temporal variability

As this programme is amongst the first dedicated X-ray monitoring campaigns for any ULX, it provides us with a new view of a poorly-explored region of ULX parameter space, namely X-ray variations over timescales of hours to weeks. During the campaign the count rate of NGC 5204 X-1 varied between $\sim 0.1 - 0.5$ count s⁻¹, with a corresponding observed luminosity range of $\sim 1.3 - 6.3 \times 10^{39}$ erg s⁻¹. The most obvious feature to look for in such data

Table 6. Varying empirical model parameters over the campaign.

Obs.	Model & parameters ^a				
	(1) Γ	kT	(3) Γ	kT	(4) kT_{in}
50-ks	2.55 ± 0.04	$0.67^{+0.08}_{-0.07}$	2.93 ± 0.05	0.17 ± 0.01	0.92 ± 0.01
Faint	$3.10^{+0.14}_{-0.13}$	$0.48^{+0.08}_{-0.07}$	$3.98^{+0.17}_{-0.16}$	0.16 ± 0.01	0.73 ± 0.01
Bright	2.35 ± 0.04	$0.60^{+0.13}_{-0.10}$	2.56 ± 0.04	0.20 ± 0.01	1.14 ± 0.01
<i>XMM</i>	2.08 ± 0.02	$1.22^{+0.09}_{-0.08}$	$2.67^{+0.04}_{-0.06}$	0.18 ± 0.01	$1.54^{+0.08}_{-0.07}$

Notes: ^a Models and parameters as per Table 3.

is a periodicity on the timescale of days. Indeed, using the B0 Ib identification of the counterpart to NGC 5204 X-1 found by Liu et al. (2004), and assuming that the star (which has $M_* = 25 M_\odot$, $R_* = 30 R_\odot$) fills its Roche lobe, Liu et al. predict orbital periods of 200-300 hours for black holes in the mass range 3-1000 M_\odot underlying NGC 5204 X-1, providing us with a testable hypothesis.

The most likely and dramatic manifestation of this periodicity would be in the form of eclipses of the X-ray source by the supergiant secondary star, as is discussed for ULXs in general by Pooley & Rappaport (2005). These authors point out that the presence of eclipses in ULX light curves could be an additional diagnostic of the mass of the black hole in the ULX, with stellar-mass black hole systems at least twice as likely to display eclipses. Promisingly, the fairly large amplitude (factor ~ 5) variability seen in NGC 5204 X-1 on timescales of days occurs between fairly consistent “high” ($\sim 0.5 \text{ count s}^{-1}$) and “low” ($\sim 0.1 \text{ count s}^{-1}$) flux states, that one might perhaps expect to see as the source goes in and out of eclipse. However, no periodic signal to support this interpretation was recovered from the data. This argues that the variability is not due to eclipsing, but may simply be due to accretion processes producing variability on the timescale of days. If this is true of many ULXs, then detecting X-ray eclipses on the timescale of their orbits (which Pooley & Rappaport note could vary from 1-150 days, even for a very limited choice of black hole/secondary star mass assumptions) may be far more difficult than simply getting round the logistical problem of acquiring X-ray monitoring data with a high observational efficiency over timescales of days.⁸

Despite the lack of a periodic signal, short-timescale (i.e. intra-observation) variability could still be a useful diagnostic of the accretion state of the ULX through standard analysis techniques, for example the calculation of the fluctuation Power Spectral Density for the ULX. However, such analyses are in practice hampered by the poor photon statistics of our data - we have too few photons for reliable PSD analyses of the short observations, and can do no better than a few 10s of seconds resolution in our light curves before becoming dominated by Poisson noise. Despite this the light curve data we do have, and the PSD of the 50 ks observation, are good enough to tell us that NGC 5204 X-1 displays no strong variability on timescales less than a few thousand seconds. On timescales longer than this NGC 5204 X-1 is varying, suggestive of a red noise PSD with its weak power at higher ($\gtrsim 10^{-3} \text{ Hz}$) frequencies swamped by statistical noise in the data.

⁸ Though we note that true extragalactic eclipsing sources may now be starting to be observed, for example with the detection of a slightly sub-ULX luminosity source in NGC 4214 with an eclipse periodicity of 3.6-hr (Ghosh et al. 2006b).

5.1.1 A comparison with GRS 1915+105

One interesting means of interpreting our temporal data is via a direct comparison with GRS 1915+105 (see Fender & Belloni 2004 for a review of the properties of this remarkable object). This source is the archetypal Galactic microquasar, and has spent much of its (to date) 15-yr outburst radiating at luminosities at or above the Eddington limit for its $\sim 14 M_\odot$ black hole (Done, Wardziński & Gierliński 2004). This would make it a ULX to an observer external to our Galaxy, hence it is potentially crucial for our understanding of ULXs as a whole. As it has a low-mass companion, King (2002) suggested that sources akin to GRS 1915+105 could explain the lower-luminosity ULXs associated with old stellar populations (such as the population of $1 - 2 \times 10^{39} \text{ erg s}^{-1}$ ULXs associated with elliptical galaxies; Irwin, Bregman & Athey 2004). A direct comparison between GRS 1915+105 and the brighter ULXs - thought to have much more massive companion stars - may therefore seem illogical. However there may be some crucial similarities, for example both types of system are thought to transfer mass through Roche lobe overflow, and possibly accrete at super-Eddington rates. Hence GRS 1915+105 may still be useful in interpreting the behaviour of brighter ULXs. For instance Goad et al. (2006) find that Ho II X-1, which is far more luminous than GRS 1915+105 (at $> 10^{40} \text{ erg s}^{-1}$) and a good IMBH candidate (Dewangen et al. 2005), shows no temporal variability over short ($< 1 \text{ hour}$) timescales during an $\sim 80 \text{ ks}$ observation. Interestingly, its light curve and PSD during this observation appear to mirror the χ -class of behaviours of GRS1915+105 (Belloni et al. 2000). Taken together with a possible mass limit derived from PSD analysis, Goad et al. argue that Ho II X-1 is a $< 100 M_\odot$ black hole accreting at very high rates, and thus behaving similarly to GRS 1915+105 in its “ χ ” (or “plateau”) state.

One simple test is to qualitatively compare the long-term light curve of GRS 1915+105 obtained from *RXTE* all-sky monitor (ASM) data (Fig. 2, Fender & Belloni 2004) to our monitoring light curve. Despite a moderate bandpass difference (0.5 – 8 keV for *Chandra* ACIS-S versus 1.5 – 12 keV for the ASM), both light curves show a similar amplitude variability, factors ~ 5 over a timescale of days. Indeed, it is plausible that if one randomly sampled the GRS 1915+105 light curve at the same rate as our NGC 5204 X-1 light curve in Fig. 1, one would find a very similar light curve. However, this similarity is not necessarily maintained over shorter timescales. In particular GRS 1915+105 spends a reasonable fraction of its time ($\sim 33 - 50\%$)⁹ displaying fairly extreme

⁹ We calculate this from Table 1 of Belloni et al. (2000). We assume that the 349 observation intervals between January 1996 and December 1997 are representative of the behaviour of GRS 1915+105, and that the χ and ϕ

short-term variability, characterised by complex, sometimes very repetitive variability patterns in its light curves with cycle times ranging from tens to thousands of seconds. These are thought to be due to limit-cycle instabilities in the inner accretion disc such that it is continually emptying and refilling (Belloni et al. 2000)¹⁰. No such behaviour is seen from NGC 5204 X-1, even though we are sensitive to variations on timescales $\lesssim 100$ seconds in our data.

What does this imply about the nature of NGC 5204 X-1? An important clue could be that GRS 1915+105 only displays its unique limit-cycle variability when it is accreting at super-Eddington rates (Done et al. 2004). This implies that this behaviour could be an observational signature of super-Eddington accretion. If so, the absence of such behaviour in NGC 5204 X-1 would imply it is accreting at a sub-Eddington rate. In this case, we must either be observing beamed X-ray emission (likely of the variety suggested by King et al. 2001) or observing isotropic emission from a larger black hole, with the peak luminosities of 6.3×10^{39} erg s⁻¹ implying a black hole mass in excess of $45M_{\odot}$. Interestingly, as most ULXs also show little or no short-term variability (cf. Swartz et al. 2004, Feng & Kaaret 2005), and certainly nothing resembling the limit-cycle variability of GRS 1915+105, this argument could imply that the vast majority of ULXs are sub-Eddington accretors.

Of course, this is reliant on the limit-cycle behaviour of GRS 1915+105 being typical of all sources accreting above the Eddington rate, and this is by no means assured. For example, there are several neutron stars that exceed the Eddington limit in our own Galaxy (including Cir X-1 at up to $10 L_{\text{Edd}}$), none of which show limit-cycle variability similar to GRS 1915+105, though Done et al. (2004) note that irradiation of the accretion flow by the boundary layer on the neutron star's surface might act as a stabilizing mechanism. Perhaps more pertinently, other Galactic black holes have reached super-Eddington states (McClintock & Remillard 2005), with no reports of similar limit-cycle variability. If we are to use the apparent absence of limit-cycle variability as an argument that ULXs are sub-Eddington accretors, then the key observation would be to catch a ULX behaving in precisely this way when it radiates at its brightest X-ray luminosities. Otherwise, the lack of such behaviour in ULXs might just serve to emphasize how unusual GRS 1915+105 actually is.

5.2 On the soft part of the X-ray spectrum

As Fig. 5 demonstrates, the soft end of our X-ray spectrum showed unusual residuals, most notably a line-like feature peaking at ~ 1 keV. Our spectral modelling showed that this feature could be described in two ways; either it is the most prominent feature deriving from the presence of a warm ($kT \sim 0.9$ keV) MEKAL optically thin thermal plasma, or it could be described by a single, broadened ($\sigma \sim 70$ eV) Gaussian line at 0.96 keV, with a relatively low equivalent width ($\sim 50 - 80$ eV). Whilst the other components of the spectral modelling were required to vary to maintain good spectral fits throughout our campaign, the contribution of this component remained the same.

states (that are present in $\sim 50\%$ of observations) will appear invariant in our observations. We note that the α , γ and δ states (a further $\sim 17\%$) may also appear as such in our comparatively low quality data.

¹⁰ In this case the limit-cycle instability is thought to be driven by cyclical changes in the balance between gas pressure and radiation pressure. This is distinct from a second form of limit-cycle instability, namely the ionised versus neutral hydrogen cycle, which dominates the long-term transient behaviour (i.e. outburst versus quiescence) in accretion discs.

So what is the origin of this feature? ULXs in which a MEKAL component models some part of their X-ray spectrum are relatively scarce (though see e.g. Terashima & Wilson 2004; Roberts et al. 2004; Dewangen et al. 2005; Feng & Kaaret 2005; Soria et al. 2006), and in some of these cases we are faced with a very soft component that is spectrally indistinguishable from a very soft accretion disc with the quality of data available. That is not the case in this observation, where an optically-thin plasma clearly provides the best explanation for the soft X-ray spectrum. This fit is driven by the feature at ~ 1 keV, similarly to the MEKAL component found to be required to fit the spectrum of NGC 4395 X-1 (SRW06; Feng & Kaaret 2005).

Feng & Kaaret (2005) argue that a soft thermal component could arise in a supernova remnant (SNR) co-located with the ULX. For this to be true, the contribution of the SNR to the X-ray flux of the ULX must always be less than (or at most equal to) the total observed flux, as a structure of light years in size cannot vary its X-ray flux on the timescale of hours to days. By examining the contribution of the MEKAL components in Models (1) & (2) to the fitted spectrum of the 50-ks observation, we can infer that the MEKAL from Model (1) contributes ~ 0.03 count s⁻¹ to the overall count rate, which is plausible given the minimum observed count rates of ~ 0.1 count s⁻¹ for NGC 5204 X-1. However, in Model (2) the MEKAL is responsible for ~ 0.16 count s⁻¹, meaning it cannot originate in a large structure like a SNR.¹¹ If the thermal component in Model (1) does originate in a SNR, we note that it cannot be very old - its temperature of ~ 0.96 keV is rather similar to the temperatures of the reverse shock components that become visible on the timescale of years - a couple of decades in recent supernovae (e.g. Immler & Lewin 2003) but somewhat higher than the $\sim 0.2 - 0.4$ keV temperatures of the fainter and older SNR population of M33 (Ghavamian et al. 2006). The fact that the X-ray flux of this component is seen to brighten by a factor ~ 5 in the eight months between the *XMM-Newton* observation and the *Chandra* programme (during which it remains constant) may be difficult to reconcile with a large structure such as an SNR, though we note that the X-ray emission of SN 1987A has been seen to evolve relatively rapidly (on the timescale of months) as its blast wave propagates outwards and hits dense clumps of ISM, causing X-ray “hotspots” to turn on (e.g. Park et al. 2004). However, in this case it is puzzling that one does not detect any bright radio emission from NGC 5204 X-1 (Körding, Colbert & Falcke 2005), as most X-ray bright recent supernovae also appear radio bright (Immler & Lewin 2003).

If the feature does not arise in an underlying SNR, where else could it originate? If we consider the Gaussian line fit, its line width of $\sim 60-80$ eV corresponds to velocities of $0.06-0.08c$ ($18000-24000$ km s⁻¹) for matter radiating a single emission line. Whilst these velocities may be plausible for the innermost regions of an accretion disc and/or a mildly relativistic outflow, in the absence of direct evidence for a relativistic origin (for example, a classic skewed line profile, or a measurement of its blue- or redshift), or indeed a good candidate for a single dominant emission line at this energy, perhaps a more realistic interpretation is that the feature originates as a blend of the Ne K and Fe L lines prominent around 0.96 keV.

¹¹ As the necessity to vary this MEKAL component conflicts with every other model showing that the soft component remains invariant as the ULX flux changes, we do not consider this model as viable for explaining the spectral changes, and so exclude it from the analysis in Section 4.3.

It is once again pertinent to raise GRS1915+105 at this point, as recent *XMM-Newton* EPIC observations have shown that it displays a remarkably similar spectral feature, namely a broad ($\sigma \sim 90$ eV) emission line at 0.97 keV, albeit with a much higher equivalent width of 5.6 keV (Martocchia et al. 2006). Whilst there are caveats attached to this detection - most notably the non-detection of a corresponding feature in simultaneous *XMM-Newton* RGS data - this finding again raises the question of whether there are at least some physical similarities between GRS1915+105 and NGC 5204 X-1. Martocchia et al. (2006) interpret the line feature as possible evidence for a photoionized disc wind (a collisionally-ionized wind is also discussed, but rejected because calculations show any such wind in GRS 1915+105 must be approaching the optically-thick regime). The same interpretation could apply to NGC 5204 X-1, though the lower equivalent width of its line requires an explanation (speculations could include the continuum level being higher relative to the wind emission, or the wind emission simply being less bright in NGC 5204 X-1 than GRS 1915+105). If so, this could be the first evidence of a photoionized disc wind contributing to the X-ray emission of a ULX.

5.3 On the overall spectral shape and its variation

In Table 3 we show five spectral models, four of which are broadly empirical and the fifth more physically-based, which can adequately describe the 50-ks *Chandra* ACIS-S spectrum of NGC 5204 X-1. We can arguably rule one fit (number 2) out. We are then left with models that (if taken at face value) variously describe (1) a compact non-thermal emitter surrounded by a near-solar metallicity thermal plasma, (3) a fairly “standard” representation of an accretion disc plus corona spectrum with a broad emission line just short of 1 keV, (4) a standard accretion disc plus soft thermal excess model with the same emission line and (5) a physical accretion disc plus corona model, again with the broad emission line. Unfortunately even with the relatively good quality of a ~ 9000 count ACIS-S spectrum we can only tell that these are all adequate descriptions of the spectral shape, and not begin to distinguish between these models in a statistical sense. We are then left to make the choice as to whether we draw our physical insight from the simpler, empirical models by comparison to the fits these models make to better understood sources, or whether we trust the insight of more physical models at the possible cost of allowing more degrees of freedom and/or potential ambiguity if the best-fitting parameters show large uncertainty ranges. Both methods have benefits and drawbacks (with opposite viewpoints outlined by Miller, Fabian & Miller 2006 and Goncalves & Soria 2006). Here, we will consider the insights provided by the physical model further.

SRW06 find that the majority of ULXs with high-quality *XMM-Newton* EPIC spectral data display a spectral break (which could also be described as a cut-off, or interpreted as an indicator of curvature) above 2 keV, which could be an important clue as to the physical nature of ULXs. These authors are not the only ones to identify such a feature in ULXs; this was firstly seen by Kubota, Done & Makishima (2002) in *ASCA* GIS data from IC 342 X-1, and more recently has been seen for other ULXs observed by *XMM-Newton*, notably the top IMBH candidates Ho IX X-1 (Dewangen, Griffiths & Rao 2006) and M82 X-1 (Agrawal & Misra 2006). This break argues against the simple IMBH model where the emission above 2 keV is dominated by a single power-law continuum representative of an optically-thin hot corona (as observed in most Galactic black hole X-ray binaries), and could indicate the presence of unusual physical processes in the system. One such ex-

planation discussed by SRW06 is the presence of an optically-thick corona. Though such fits require the seeding of the corona by a disc with an IMBH-like temperature, SRW06 refer to two models (Zhang et al. 2000; Done & Kubota 2006) viably describing very high accretion rate systems - with no requirement for an IMBH - that could explain both the apparently cool disc emission, and the optically thick corona (see also Kuncic & Bicknell 2004 for a similar model).

Our physical model (5) describes the continuum emission of NGC 5204 X-1 as an optically thick corona seeded by a cool disc, consistent with the modelling of other ULXs from *XMM-Newton* data.¹² Importantly, the *Chandra* data is of sufficient quality to demonstrate that this solution is preferred at the 3σ level to an optically-thin solution (with the latter also taking an implausibly low disc temperature of 20 eV). Perversely though, the *Chandra* data alone is not of good enough quality to rule out an unbroken power-law above 2 keV, with the simple power-law versus broken power-law test of SRW06 inconclusive in this instance. This is perhaps unsurprising given that there are only three data points above 5 keV in the *Chandra* data, and that models including a hard power-law [(1), (3)] do provide good fits to the data. In this case we can turn to the *XMM-Newton* data for this ULX for confirmation, which as SRW06 demonstrate does indeed show a significant break feature at ~ 5 keV.

However, if we are to maintain any faith in this physical model, its parameters must vary in a physical way throughout the monitoring programme. Our modelling of data taken from within the 50-ks observation, and from the full monitoring programme, show that the hardening of the spectra with increasing flux (graphically demonstrated by the hardness ratios of Fig. 4) can be modelled predominantly as an increase in the temperature of the corona as the ULX luminosity increases, with additional changes in the seed disc temperature occurring over timescales of days. This trend is not just seen in the *Chandra* data; as we have shown, an *XMM-Newton* observation is also consistent with this behaviour. Interestingly, this echoes the behaviour of XTE J1550-564 in a subset of its very high state that Kubota & Done (2004) describe as a “strong very high state”. This state is characterised by strong Comptonisation from a cool (albeit in this case still 10 - 30 keV) corona, and unusually low disc temperatures for its luminosity (~ 0.5 keV against an expectation of ~ 1 keV for that luminosity in the high/soft state). In this state the temperature of the corona does indeed seem to track the luminosity of the system (see Fig. 5 of Kubota & Done 2004). We therefore speculate that NGC 5204 X-1 is in a more extreme version of this strong very high state, characterised by a cooler disc and a thicker corona. We further speculate that this thicker corona could be fueled by the extreme mass transfer rates possible for ULXs if they are stellar-mass black holes accreting from young, massive stars as described by Rappaport, Podsiadlowski & Phahl (2005). Indeed, Done & Kubota (2006) note that this state has the characteristics to explain the X-ray spectra of many ULXs without the need to resort to IMBHs.

We therefore conclude that the optically-thick solution remains a physically plausible model for this ULX, though we caution that it is by no means an unique solution for this data. As reported in previous work, this could again mean that we are looking at a very high accretion rate stellar-mass (or slightly larger)

¹² Obviously we have a second, line-like component in our spectral fit. For the purposes of this discussion we treat its origin as separate from the underlying continuum.

black hole. In this state it could share some similarities with GRS 1915+105, though we have shown that limit-cycle variability does not appear to be one of them. A possible outflow identified by the soft, broad emission line-like component identified at ~ 0.96 keV is however one potential similarity. Whilst the possible detection of an optically thick corona continues a current trend for bright ULXs (and should not be a surprise given SRW06 detected a similar spectrum in *XMM-Newton* data for this ULX), the detection of the broad line feature is unexpected. The presence of this line is certainly very unusual when compared to the range of ULX characteristics reported to date, and as such it should be fully investigated by future studies, in particular by utilising the reflection grating spectrometers on *XMM-Newton* to probe the composition of this feature.

6 CONCLUSION

We have reported the results of a two-month monitoring programme of NGC 5204 X-1, over timescales of days to weeks. We detect no periodic variability, and the source shows little variability at all on timescales less than an hour, though it varies by factors of ~ 5 over a few days. This flux variation is accompanied by spectral changes, in the sense that the source spectrum becomes harder as the flux increases. The spectrum of the ULX is composed of two main features: a broad emission line at ~ 0.96 keV, and a smooth underlying continuum, that can together be described by a variety of multi-component models. One of these models describes a continuum originating in an optically-thick corona, consistent with other recent results for ULXs, that could describe an extreme form of a strongly Comptonised very high state that is seen in Galactic black hole X-ray binaries. The spectral variations appear consistent with the known behaviour of sources in this state. This model does not require an IMBH to power the ULX. Of course, this is not the same as ruling out the presence of an IMBH in this system.

The insights gained from studying variations in the X-ray spectra and temporal characteristics of Galactic black holes over timescales from milliseconds to years have been immense, and have been facilitated by the unique capabilities of the *RXTE* satellite (McClintock & Remillard 2006 and references therein). Such studies cannot currently be done for any single extragalactic ULX, with the exception of M82 X-1 (Kaaret, Simet & Lang 2006a,b), and even that study is limited by effects such as the possible confusion of multiple ULXs in the centre of M82. For the remaining fainter sources we are currently constrained to small monitoring campaigns using *XMM-Newton* and *Chandra*, which have been surprisingly rare to date given the potential physical insights they can offer. Future, sensitive all-sky monitors with arcminute resolution such as *Lobster* (Fraser et al. 2002) will at least offer a reasonable monitoring platform for the brightest ULXs so that we can finally examine the details of their day-to-day behaviour. Until then, improvement in our insights into the physical processes of ULXs - and hence their underlying nature - will continue to rely on obtaining deeper single observations, or more monitoring of the type described in this paper.

ACKNOWLEDGMENTS

We would like to thank an anonymous referee for helping us to improve this paper. TPR gratefully acknowledges support from the UK Particle Physics and Astronomy Research Council (PPARC). The authors would also like to thank Simon Vaughan for his advice on temporal analyses, and Chris Done for discussions on Galactic black holes. This work is in part based on observations obtained

with *XMM-Newton*, an ESA science mission with instruments and contributions directly funded by ESA member states and the USA (NASA).

REFERENCES

- Abramowicz M.A., Kluźniak W., McClintock J.E., Remillard R.A., 2004, *ApJ*, 609, L63
- Agrawal V.K., Misra R., 2006, *ApJ*, 638, L83
- Bauer F.E., Brandt W.N., Sambruna R.M., Chartas G., Garmire G., Kaspi S., Netzer H., 2001, *AJ*, 122, 182
- Bauer M., Pietsch W., 2005, *A&A*, 442, 925
- Begelman M.C., 2002, *ApJ*, 568, L97
- Belloni T., Klein-Wolt M., Méndez M., van der Klis M., van Paradijs J., 2000, *A&A*, 355, 271
- Ciliegi P., Elvis M., Wilkes B.J., Boyle B.J., McMahon R.G., 1997, *MNRAS*, 284, 401
- Colbert E.J.M., Mushotzky R.F., 1999, *ApJ*, 519, 89
- Colbert E.J.M., Ptak A.F., 2002, *ApJS*, 143, 25
- Cropper M., Soria R., Mushotzky R.F., Wu K., Markwardt C.B., Pakull M., 2004, *MNRAS*, 349, 39
- David L.P., Jones C., Forman W., Murray S.S., 2005, *ApJ*, 635, 1053
- Dewangan G.C., Griffiths R.E., Choudhury M., Miyaji T., Schurch N.J., 2005, *ApJ*, 635, 198
- Dewangan G.C., Griffiths R.E., Rao A.R., 2006, *ApJ*, 641, L125
- Dewangan G.C., Miyaji T., Griffiths R.E., Lehmann I., 2004, *ApJ*, 608, L57
- Dewangan G.C., Titarchuk L., Griffiths R.E., 2006, *ApJ*, 637, L21
- Done C., Kubota A., 2006, *MNRAS*, in press (astro-ph/0511030)
- Done C., Wardziński G., Gierliński M., 2004, *MNRAS*, 349, 393
- Ebisawa K., Zycki P., Kubota A., Mizuno T., Wataria K., 2003, *ApJ*, 597, 780
- Fabbiano G., 1989, *ARA&A*, 87, 27
- Fabbiano G., Zezas A., King A.R., Ponman T.J., Rots A., Schweizer F., 2003, *ApJ*, 584, L5
- Fender R., Belloni T., 2004, *ARA&A*, 42, 317
- Feng H., Kaaret P., 2005, *ApJ*, 633, 1052
- Fiorito R., Titarchuk L., 2004, *ApJ*, 614, L113
- Foschini L., Rodriguez J., Fuchs Y., Ho L.C., Dadina M., Di Cocco G., Courvoisier T.J.-L., Malaguti G., 2004, *A&A*, 416, 529
- Fraser G., et al., 2002, *Proc. SPIE*, 4497, 115
- Ghavamian P., Blair W.P., Long K.S., Sasaki M., Gaetz T.J., Plucinsky P.P., 2005, *AJ*, 130, 539
- Ghosh K.K., Finger M.H., Swartz D.A., Tennant A.F., Wu K., 2006a, *ApJ*, 640, 459
- Ghosh K.K., Rappaport S., Tennant A.F., Swartz D.A., Pooley D., Madhusudhan N., 2006b, *ApJ*, in press (astro-ph/0604466)
- Goad M.R., Roberts T.P., Knigge C., Lira P., 2002, *MNRAS*, 335, L67
- Goad M.R., Roberts T.P., Reeves J., Uttley P., 2006, *MNRAS*, 365, 191
- Goncalves A., Soria R., 2006, *MNRAS*, in press (astro-ph/0606273)
- Grimm H.-J., Gilfanov M., Sunyaev R., 2003, *MNRAS*, 339, 793
- Immler S., Lewin W.H.G., 2003, In: *Supernovae and Gamma-ray Bursters*, Ed. K. Weiler, Springer-Verlag (New York), p91
- Irwin J.A., Bregman J.N., Athey A.E., 2004, *ApJ*, 601, L143
- Jenkins L.P., Roberts T.P., Warwick R.S., Kilgard R.E., Ward M.J., 2004, *MNRAS*, 349, 404
- Kaaret P., Prestwich A., Zezas A., Murray S., Kim D.-W., Kilgard R., Schlegel E., Ward M., 2001, *MNRAS*, 321, L29
- Kaaret P., Simet M.G., Lang C.C., 2006a, *Sci*, 311, 491
- Kaaret P., Simet M.G., Lang C.C., 2006b, *ApJ*, in press (astro-ph/0604029)
- Kalogera V., Henninger M., Ivanova N., King A.R., 2004, *ApJ*, 603, L41
- King A., 2002, *MNRAS*, 335, L13
- King A., 2004, *MNRAS*, 347, L18
- King A., Davies M.B., Ward M.J., Fabbiano G., Elvis M., 2001, *ApJ*, 552, L109
- King A., Pounds K.A., 2003, *MNRAS*, 345, 657
- Körding E., Colbert E., Falcke H., 2005, *A&A*, 436, 427
- Körding E., Falcke H., Markoff S., 2002, *A&A*, 382, L13

- Krauss M., Kilgard R., Garcia M., Roberts T.P., Prestwich A., 2005, ApJ, 630, 228
- Kubota A., Done C., 2004, MNRAS, 353, 980
- Kubota A., Done C., Makishima K., 2002, MNRAS, 337, L11
- Kubota A., Mizuno T., Makishima K., Fukazawa Y., Kotoku J., Ohnishi T., Tashiro M., 2001, ApJ, 547, L119
- Kuncic Z., Bicknell G.V., 2004, ApJ, 616, 669
- Liu J.-F., Bregman J.N., 2005, ApJS, 157, 59
- Liu J.-F., Bregman J.N., Irwin J., Seitzer P., 2002, ApJ, 581, L93
- Liu J.-F., Bregman J.N., Lloyd-Davies E., Irwin J., Espaillat C., Seitzer P., 2005, ApJ, 621, L17
- Liu J.-F., Bregman J.N., Seitzer P., 2004, ApJ, 602, 249
- Makishima K. et al., 2000, ApJ, 535, 632
- Martocchia A., Matt G., Belloni T., Feroci M., Karas V., Ponti G., 2006, A&A, 448, 677
- McClintock J.E., Remillard R.A., 2006, in: "Compact Stellar X-ray Sources", eds. Lewin W.H.G. and van der Klis M., Cambridge University Press (Cambridge), p. 157
- Miller J.M., Fabbiano G., Miller M.C., Fabian A.C., 2003, ApJ, 585, L40
- Miller J.M., Fabian A.C., Miller M.C., 2004, ApJ, 607, 931
- Miller J.M., Fabian A.C., Miller M.C., 2006, ApJ, submitted (astro-ph/0512552)
- Miller M.C., Colbert E.J.M., 2004, Int. J. Mod. Phys. D, 13, 1
- Mucciarelli P., Casella P., Belloni T., Zampieri L., Ranalli P., 2006, MNRAS, 365, 1123
- Mukai K., Still M., Corbet R.H.D., Kuntz K.D., Barnard R., 2005, ApJ, 634, 1085
- Park S., Zhekov S.A., Burrows D.N., Garmire G.P., McCray R., 2004, ApJ, 610, 275
- Pooley D., Rappaport S., 2005, ApJ, 634, L85
- Portegies Zwart S.F., Baumgardt H., Hut P., Makino J., McMillan S.L.W., 2004, Nature, 428, 724
- Rappaport S.A., Podsiadlowski Ph., Pfahl E., 2005, MNRAS, 356, 401
- Roberts T.P., Goad M.R., Ward M.J., Warwick R.S., O'Brien P.T., Lira P., Hands A.D.P., 2001, MNRAS, 325, L7
- Roberts T.P., Warwick R.S., 2000, MNRAS, 315, 98
- Roberts T.P., Warwick R.S., Ward M.J., Goad M.R., 2004, MNRAS, 349, 1193
- Roberts T.P., Warwick R.S., Ward M.J., Goad M.R., Jenkins L.P., 2005, MNRAS, 357, 1363
- Soria R., Cropper M., Pakull M., Mushotzky R., Wu K., 2005, MNRAS, 356, 12
- Soria R., Kuncic Z., Broderick J.W., Ryder S.D., 2006, MNRAS, in press (astro-ph/0606080)
- Soria R., Motch C., Read A.M., Stevens I.R., 2004, A&A, 423, 955
- Stark A., Gammie C.F., Wilson R.W., Bally J., Linke R.A., Heiles C., Hurwitz M., 1992, ApJS, 79, 77
- Stobbart A., Roberts T.P., Wilms J., 2006, MNRAS, 368, 397 (SRW06)
- Strickland D.K., Colbert E.J.M., Heckman T.M., Weaver K.A., Dahlem M., Stevens I.R., 2001, ApJ, 560, 707
- Strohmayer T.E., Mushotzky R.F., 2003, ApJ, 586, L61
- Swartz D.A., Ghosh K.K., Tennant A.F., Wu K., 2004, ApJS, 154, 519
- Terashima Y., Wilson A., 2004, ApJ, 601, 735
- Uttley P., McHardy I.M., Papadakis I.E., 2002, MNRAS, 332, 231
- van der Klis M., 1997, in G.J. Babu, E. D. Feigelson eds., *Statistical Challenges in Modern Astronomy II*, Springer-Verlag (New York), p321
- Watarai K., Mizuno T., Mineshige S., 2001, ApJ, 549, L77
- Weisskopf M.C., Wu K., Tennant A.F., Swartz D.A., Ghosh K.K., 2004, ApJ, 605, 360
- Wilms J., Allen A., McCray R., 2000, ApJ, 542, 914
- Zhang S.N., Cui W., Chen W., Yao Y., Zhang X., Sun X., Wu X., Xu H., 2000, Sci, 287, 1239